Defect Detection in Textured Materials Using Gabor Filters

Ajay Kumar, *Member, IEEE,* and Grantham K. H. Pang, *Senior Member, IEEE*

Abstract—This paper investigates various approaches for automated inspection of textured materials using Gabor wavelet features. A new supervised defect detection approach to detect a class of defects in textile webs is proposed. Unsupervised web inspection using multichannel filtering scheme is investigated. A new data fusion scheme to multiplex the information from the different channels is proposed. Various factors interacting the tradeoff for performance and computational load are discussed. This scheme establishes high computational savings over the previously proposed approaches and results in high quality of defect detection. Final acceptance of visual inspection systems depends on economical aspects as well. Therefore, a new low-cost solution for fast web inspection is also included in this paper. The experimental results conducted on real fabric defects for various approaches proposed in this paper confirm their usefulness.

Index Terms—Computer vision, defect detection, Gabor filters, Gabor wavelets, industrial automation, multichannel filtering, quality assurance, textile industry.

I. INTRODUCTION

VISION-BASED inspection of industrial products offers low-cost, high-speed, and high-quality detection of defects. Some of the most challenging industrial inspection problems deal with the textured materials such as textile web, paper, and wood. The inspection problem encountered in textured materials become texture analysis problems at microscopic levels. Textured materials take many forms and while there is a remarkable similarity in overall automation requirements for visual inspection, the cost-effective solutions are application specific and generally require extensive research and development efforts [1]. Automated visual inspection of textured materials, woven or nonwoven, such as paper [2], steel roll [3], wood [4], [5], carpet [6], textile [7]–[23], etc., has been used for defect detection and quality assurance.

In general, an image of woven fabric sample can be regarded as a typical textured image. The detection of local fabric defects is one of the most intriguing problems in computer vision and

has received much attention over the years [7]–[23]. This paper focuses on this problem and proposes some new techniques to address the problem

In textile looms, the fabric produced is typically 8–10-ft wide and rolls out at the speed of 5–6 ft/s. The fabric produced is packed into rolls and later unrolled for inspection on the inspection table. The major reasons for this offline inspection is the slow speed of production, which is insufficient to keep an inspector occupied, and the relatively hostile environment. The majority of automated inspection systems currently available in the market are offline. Typical of these is the I-TEX inspection system available from Elbit Vision Systems [8], which can detect fabric defects up to a speed of 100 m/min. Many other web inspection systems available from commercial vendors are tailored to detect and locate defects accurately while maximizing the throughput. Each of these inspection systems has its own limitations and defect detection is limited to a certain range of defects. Fabric defect detection is still a topic of considerable research and researchers have proposed different algorithm to reduce the cost, and improve the throughput and range of defects that can be detected.

A. Prior Work

Various approaches for fabric defect detection have been proposed in the past two decades [7]–[23]. The texture analysis techniques for fabric defect detection are intuitively appealing, because they allow us to capture texture features, which are statistically used to segment fabric defects. Gray-level texture features extracted from co-occurrence matrix [9], mean and standard deviations of subblocks [10], autocorrelation of subimages [11], and Karhunen–Loève (KL) transform [12] have been used for the segmentation of local fabric defects. Cohen *et al.* [13] have characterized the fabric texture using the Gauss Markov random field (GMRF) model and the textile web inspection process is treated as a hypothesis-testing problem on the statistics derived from this model. Campbell *et al.* [14] use model-based clustering to segment defects from the denim fabric.

The fabric texture exhibits a high degree of periodicity and, hence, Fourier-domain features have been used for the detection of fabric defects [15], [16]. Since the Fourier bases are of infinite length, the contribution from each of the spectral components is difficult to quantify. Therefore, Fourier analysis is not suitable for detection of local defects. Instead, detection of local fabric defects requires multiresolution decomposition of fabric images across several scales. A feature vector composed of significant features at each scales is used for the identification of defects. Such a multiresolution analysis of fabric using Discrete wavelet

(a)   (b)
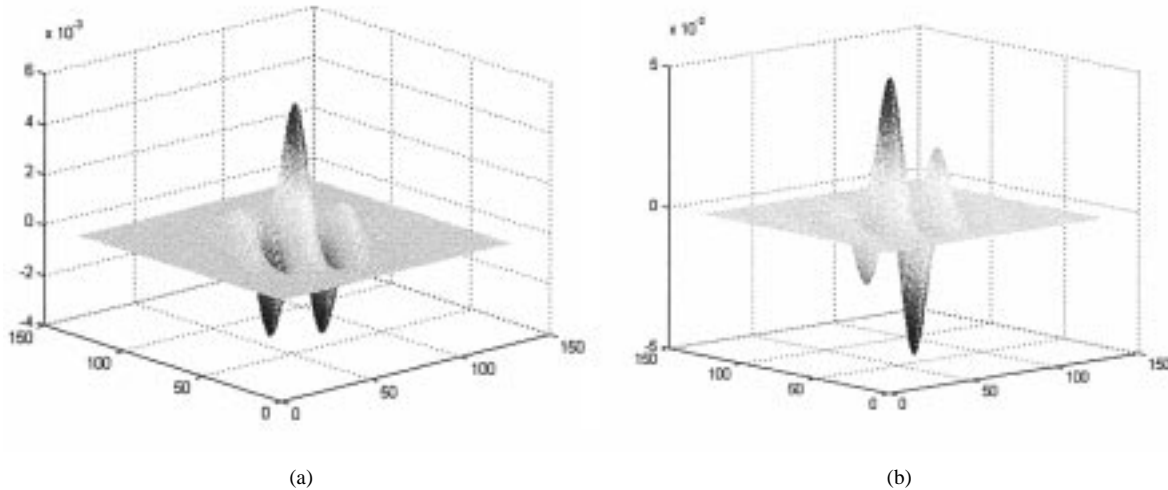
Fig. 1.   Perspective view of (a) real and (b) imaginary components of a typical Gabor function in spatial domain.

transform (DWT) has been detailed in [17]–[19]. Jasper *et al.* [20] use texture-adapted wavelet bases whose response is close to zero for normal fabric texture and significantly different for fabric defect, thereby enabling detection. Escofet *et al.* [21] use multiscale Gabor filters for textile web defect detection. Ajay and Pang [22] have demonstrated fabric defect detection using only real Gabor functions.

B. Present Work

In this paper, fabric defect detection using Gabor filters is further investigated. One common technique to implement multiresolution analysis is to use wavelet transforms. However, wavelet bases are shift invariant and, therefore, it is difficult to characterize a texture pattern from the wavelet coefficients since the wavelet descriptors depend on pattern location [24]. Gabor filters can also decompose the image into components corresponding to different scales and orientations. Gabor filters achieve optimal joint localization in spatial and spatial frequency domain [25] and, therefore, have been used extensively for texture analysis [26]–[29] and document analysis [30], [31], and object detection [32].

Although researchers have not agreed on a precise definition of texture, several definitions have been proposed in the literature [33], [34]. Many textures can be modeled as a collection of similar, not necessarily identical, primitive objects called *textels*. In uniform textures, the *textels* are identical and arranged in repeating pattern with a constant displacement of Δx along the x axis and Δy along the y axis. Dunn *et al.* [35], [36] have found that when a texture contains *textels* not arranged in square lattice ($\Delta x \neq \Delta y$), asymmetric Gabor filters are useful. The *textel* spacing (Δx, Δy) for real fabric samples is often not arranged in square lattice. This can be due to the presence of stochastic turf/perturbations on the fabric surface, and/or due to the underlying structure of the fabric itself as in the case of many twill weave fabrics. The fabric defect detection using asymmetric Gabor filters is investigated in this paper. For supervised defect detection, no effective systematic method existed previously [22] for automatically selecting the desired Gabor filter.

The main contributions of this paper [37] are summarized as follows.

1) A new supervised defect detection scheme to detect a class of fabric defects is proposed.
2) A new multichannel filtering scheme for unsupervised fabric defect detection using a class of self-similar Gabor functions [27] is presented. As detailed in Section IV-G, this scheme differs from existing techniques in five crucial ways.
3) A new, low-cost solution for the web inspection using only the imaginary part of the Gabor function is presented.

The organization of this paper is as follows. In Section II, a review of Gabor filters is presented; the bank of Gabor filters used for power spectrum sampling of the image is introduced. In Section III, supervised defect detection to detect a class of fabric defects is described. In Section IV, unsupervised defect detection is described. This section includes a discussion on the proposed multichannel filtering scheme and comparison of this scheme with prior work [21]. In Section V, experimental results from the proposed low-cost inspection scheme using imaginary Gabor function are reported, which is followed by conclusions in Section VI.

II. GABOR FUNCTION

In the spatial domain, the Gabor function is a complex exponential modulated by a Gaussian function. The Gabor function forms a complete but a nonorthogonal basis set and its impulse response in the two–dimensional (2-D) plane has the following general form [27], [28]:

$$f(x, y) = \frac{1}{2\pi\sigma_x\sigma_y} \exp\left[-\frac{1}{2}\left(\frac{x^2}{\sigma_x^2} + \frac{y^2}{\sigma_y^2}\right)\right] \exp(2\pi j u_0 x)$$

(1)

where u_0 denotes the radial frequency of the Gabor function. The space constants σ_x and σ_y define the Gaussian envelope along the x and y axes. Fig. 1 shows the perspective plot of a typical Gabor filter in the spatial domain. In the frequency

domain, the Gabor function acts as a bandpass filter and the Fourier transform of $f(x, y)$ is given by

$$F(u, v) = \exp\left\{-\frac{1}{2}\left[\frac{(u - u_0)^2}{\sigma_u^2} + \frac{v^2}{\sigma_v^2}\right]\right\} \quad (2)$$

where

$$\sigma_u = \frac{1}{2\pi\sigma_x} \quad \text{and} \quad \sigma_v = \frac{1}{2\pi\sigma_y}.$$

A class of self similar-functions, referred to as Gabor wavelets,[1] which have been used for texture analysis [27], will be considered in this work. Using (1) as the mother Gabor wavelet, the self-similar filter bank can be obtained by appropriate dilation and rotation of $f(x, y)$ through the generating function

$$f_{pq}(x, y) = \alpha^{-P} f(x', y') \quad (3)$$

where

$$x' = \alpha^{-P}(x\cos\theta_q + y\sin\theta_q)$$
$$= \alpha^{-P}(-x\sin\theta_q + y\cos\theta_q),$$
$$\alpha > 1; \quad p = 1, 2, \ldots, S; \quad q = 1, 2, \ldots, L.$$

The integer subscripts p and q represent the index for scale (dilation) and orientation (rotation), respectively. S is the total number of scales and L is the total number of orientations in the self-similar Gabor filter bank. For each orientation q, the angle θ_q is given by

$$\theta_q = \frac{\pi(q - 1)}{L}, \qquad q = 1, 2, \ldots, L. \quad (4)$$

The scale factor α^{-P} ensures that the energy $E_{pq} = \int_{-\infty}^{\infty}\int_{-\infty}^{\infty}|f_{pq}(x, y)|^2 \, dx \, dy$ is independent of p [29]. Thus, all the filters in the Gabor filter bank have the same energy, irrespective of their scale and orientation. In most cases [21], [22], [28], [36], a reasonable design choice is to select circularly symmetric Gabor filters, i.e., $\sigma_x = \sigma_y$. However, as discussed in Section I-A, asymmetric Gabor filters ($\sigma_x \neq \sigma_y$) can be useful for real fabric textures. As illustrated in [27], the following formulas ensure that the half-peak magnitude responses of adjacent asymmetric filters touch each other (Fig. 6):

$$\alpha = \left(\frac{f_h}{f_l}\right)^{-(1/(S-1))}$$
$$\sigma_x = \frac{\sqrt{2\ln 2}(\alpha + 1)}{2\pi f_h(\alpha - 1)}$$
$$\sigma_y = \left[2\ln 2 - \left(\frac{2\ln 2}{2\pi\sigma_x f_h}\right)^2\right]^{1/2}$$
$$\cdot\left[2\pi\tan\left(\frac{\pi}{2L}\right)\left(f_h - 2\ln\left(\frac{1}{4\pi^2\sigma_x^2 f_h}\right)\right)\right]^{-1} \quad (5)$$

[1]The Gabor function do not exactly satisfy the requirements that the wavelet be admissible and progressive [27], [29]. However, in the context of representing a class of self-similar functions, this term is used.

where $u_0 = f_h$, and f_l and f_h are the lowest and highest frequencies of interest. A bank of self-similar Gabor filters formed by rotation (varying q) and dilation (varying p) of the basic Gabor filter (1) is used to perform power spectrum sampling of the inspection images.

Each of the complex Gabor filters has the real (even) and imaginary (odd) parts that are conveniently implemented as the spatial mask of $M \times M$ sizes. In order to have a symmetric region of support, M is preferred to be an odd number. For a given input image $I(x, y)$, the magnitude of filtered image $I_{pq}(x, y)$ is obtained by using Gabor filter $f_{pq}(x, y)$ as follows:

$$I_{pq}(x, y) = \left\{[f_{pq}(x, y)_e * I(x, y)]^2\right.$$
$$\left. + [f_{pq}(x, y)_o * I(x, y)]^2\right\}^{1/2} \quad (6)$$

where "$*$" denotes 2-D convolution operation, and $f_{pq}(x, y)_e$ and $f_{pq}(x, y)_o$ represent the even and odd parts of the Gabor filter separated from (3).

III. SUPERVISED DEFECT DETECTION

Segmentation of a similar class of local fabric defects with *a priori* knowledge about the orientation and size of a sample defect can be regarded as supervised defect segmentation [22], [37]. When the approximate orientation and size of defects are known, the power spectrum-sampling of the re spatial-frequency plane is not necessary. In such cases, he segmentation has been achieved with only one Gabor filter, from the Gabor filter bank that can provide best discrimination of texture features against the defects. The encouraging results in [22] have stressed the need for a heuristic algorithm that can automatically select a Gabor filter to detect a class of fabric defects. In order to choose the best Gabor filter, a cost function that can represent an appropriate measure of discrimination of texture features against that of defects has to be selected. The cost function used in [28] has been found suitable and used in the proposed algorithm. A Gabor filter is said to represent a defect if, on average, it produces higher outputs for regions corresponding to defect as compared with other defect-free regions of the image. The following section describes a heuristic algorithm to select the best representative Gabor filter from the bank of Gabor filters to detect a class of fabric defects.

A. Filter Selection Algorithm

A bank of $S \times L$ Gabor filters described in Section II, with S scales ($p = 1, \ldots, S$) and L orientations ($q = 1, \ldots, L$) is investigated for supervised defect detection. A real fabric image sample with a defect, which can best represent the class of fabric defects to be detected, is chosen. This image is divided into K nonoverlapping square (in our case) regions of size $l \times l$ pixels. Each of the $i = 1, 2, \ldots, S \times L$ Gabor filters in the filter bank is applied to each of the $k = 1, 2 \cdots K$ regions and a filtered output $I_{pq}(x, y)$ using equation (6) is obtained. The average output for every ith filter in the region $k = 1, 2, \ldots, K$ is obtained as follows:

$$D_k^i = \frac{1}{(l \times l)} \sum_{(x, y)\in k} I_{pq}(x, y). \quad (7)$$

For every filter i, the maximum average output $D_{\max}^i$ and the minimum average output $D_{\min}^i$ among all of the $k = 1, 2, \ldots, K$ regions is determined. A cost function $J(i)$, which is designated as the normalized difference of two outputs, is calculated for every filter in the filter bank

$$J(i) = \left(\frac{D_{\max}^i - D_{\min}^i}{D_{\min}^i} \right). \tag{8}$$

The filter $f(x, y)_{rp}$ that gives the highest cost function J_{rp} is chosen as the best representative filter to detect a class of fabric defects under consideration

$$J_{rp} = \max_{1 \leq i \leq S \times L} \{J(i)\}. \tag{9}$$

The image under investigation is filtered with this filter $f(x, y)_{rp}$ corresponding to the highest cost function J_{rp} in (9). The magnitude of this filtered image is obtained using (6) and is subjected to thresholding operation to segment the defects.

B. Thresholding

The thresholding limit is determined from a reference or defect-free fabric image. This reference image is filtered with Gabor filter $f(x, y)_{rp}$ and the magnitude of filtered image $R(x, y)$ is obtained. From this filtered image, the sholding limit is obtained as follows:

$$\psi_{th} = \max_{x, y \in W} |R(x, y)| \tag{10}$$

where "W" is a window centered at the image. Thus, he threshold value ψ_{th} is the maximum value of gray levels, within a window "W," in the image $R(x, y)$ obtained from the reference image. The window size is chosen to avoid any possible distortion effects from the image due to discontinuities at the border. In this paper, the window size is obtained by removing ten pixels (*ad hoc*) from each side of the image $R(x, y)$. The magnitude of threshold value ψ_{th} is such that the unwanted spectral components from the fabric texture are completely isolated from the output binary image.

C. Experiment and Results

Each of the filters in the filter bank is implemented as a 9×9 convolution mask for each of its real and imaginary components. The highest frequency of the filter in the filter bank $f_h = 1/2$ is empirically selected. As in [27], the filters were placed one octave apart and, thus, $f_l = 1/16$ for the Gabor filters distributed at four scales. The images of twill weave fabric samples were acquired under backlighting condition and covered 1.28×1.28 in^2 area of fabric sample. The acquired images were digitized into 256×256 pixels, with 8-bit resolution (256 gray levels). Each of these images was divided into $K = 16$ nonoverlapping regions of 64×64 pixels. The Gabor filter selected on the basis of the algorithm described in Section III-A successfully detected the defects in fabric samples. Segmentation results for the fabric samples having defects *big-knot*, *wrong-draw*, *netting-multiplies*, and *mispick* are reproduced here.

Fig. 2 shows the plot of cost function $J(i)$ for the different fabric samples shown in Fig. 3. The numbering scheme for
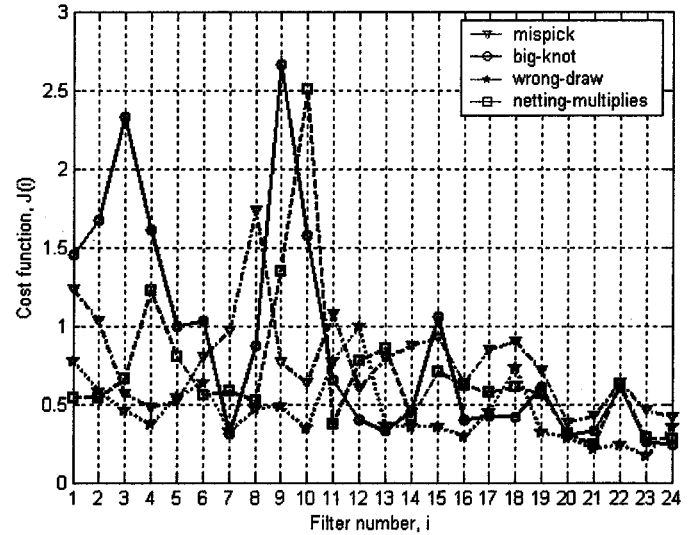

Fig. 2. Selection of best representative filter for supervised defect segmentation.

Gabor filters marked on the absicca of this plot is as follows: filter numbers 1–6 are for filters with $p = 1$ and $q = 1, \ldots, 6$ and, 7–13 are for $p = 2$ and $q = 1, \ldots, 6$, and similarly for the rest. As seen from this graph, image samples with defect *big-knot* shown in Fig. 3(a), achieves the peak of its cost function for Gabor filter number 9 ($p = 2, q = 3$). Gabor filter number 12 ($p = 2, q = 6$) achieved the peak of the cost functions for the detection of fabric defect *wrong-draw* shown in Fig. 3(d). Similarly, the fabric sample in Fig. 3(g) with defect *netting-multiplies* achieves its peak at filter number 10 ($p = 2, q = 4$) and defect *mispick* at filter number 8 ($p = 2, q = 2$). These four Gabor filters were applied to their respective fabric samples and the filtered images are shown in Fig. 3(b), (e), (h), and (k).

The filtered images were thresholded with a thresholding limit computed from the defect-free fabric sample and the defect can be seen as segmented in the thresholded images shown in corresponding Fig. 3(c), (f), (i), and (l). The Gabor filters selected with the proposed scheme were found to be robust and can segment similar kind of defects at different positions on a textile web. An example of this is reproduced here. Fig. 4(a) and (d) shows two different image samples with the defect *mispick*; the best filter selected for the segmentation of defect in Fig. 3(j) is applied to these image samples. The segmented defect can be observed in Fig. 4(c) and (f).

D. Discussion

The heuristic algorithm used to choose the best representative Gabor filter is suitable for local *rather than* global defect in the image. If the defect in the inspection image is global, i.e., it occupies most of the image, then $D_{\max}^i$ and $D_{\min}^i$ for the filters will be approximately same. In such case, the magnitude of the peak of the cost function will be smaller and reliable defect segmentation will not be achieved. The size of nonoverlapping regions ($l \times l$) should be sufficient to cover defect-free and defect regions separately. Another alternative of using nonoverlapping regions is to compute $D_{\max}^i$ and $D_{\min}^i$ in a finite region (for
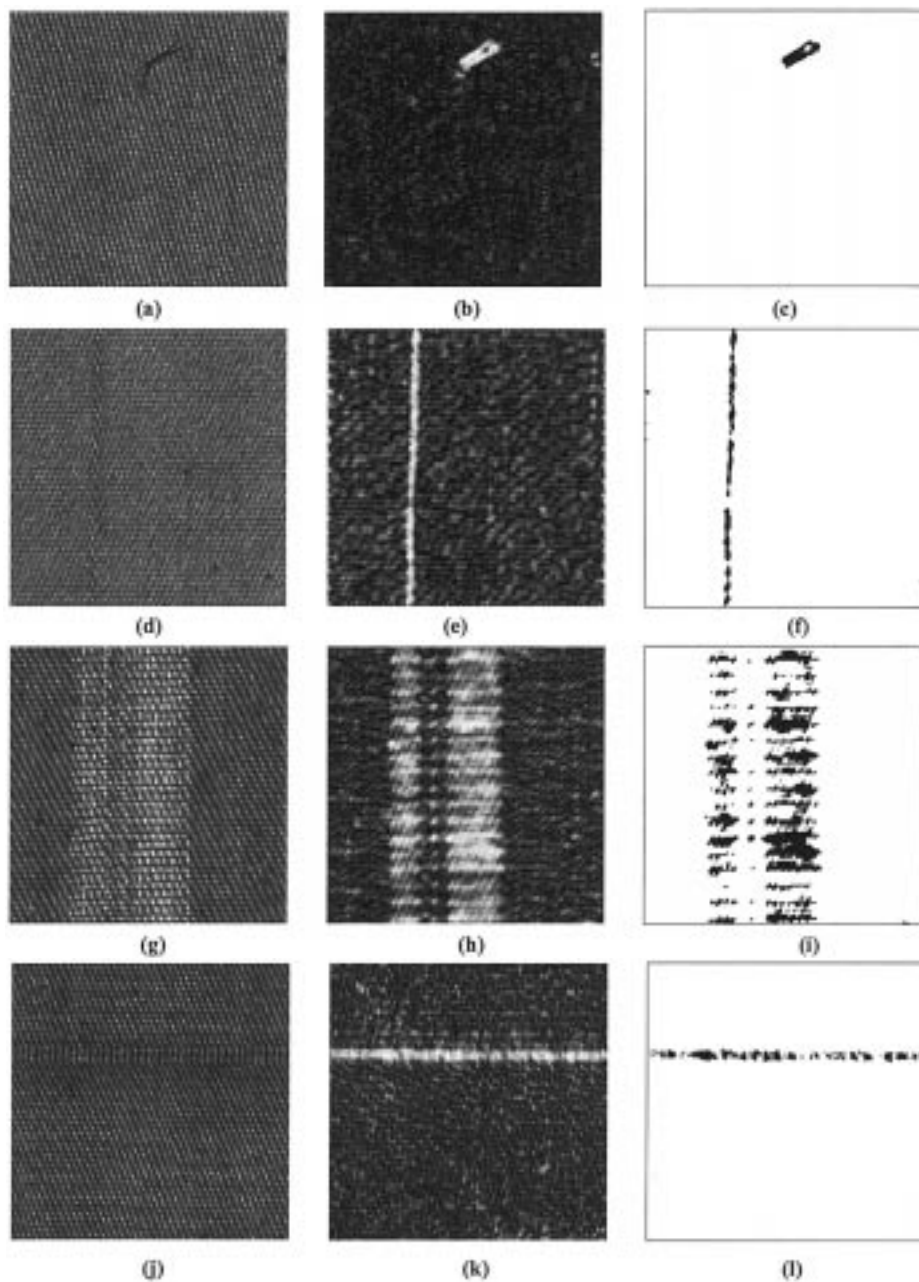
Fig. 3. Fabric samples with defect *big-knot*, *wrong-draw*, *netting-multiplies*, and *mispick* in (a), (d), (f), and (j) respectively; corresponding filtered image with the best representative Gabor filter in (b), (e), (h), and (k); segmented defects in (c), (f), (i), and (l).

example, $l \times l$) for every Gabor filter at randomly sampled locations inside the image. Since the location and the size of real fabric defect varies randomly, the finite nonoverlapping regions were preferred as this is also computationally simpler.

Optimal Gabor filters based on decision theoretic formulations can also be designed to detect a class of fabric defects. The selection of an optimal Gabor filter involves the determination of four parameters $(u, v, \sigma_x, \sigma_y)$, which define the center frequency and the bandwidth of the filter, which are optimal in the sense that the resulting Gabor filter maximizes a selected cost function. As in [36], the bandwidth (σ_x, σ_y) can be determined heuristically, and the center frequency (u, v) can be found by essentially an exhaustive search of all the possible center frequencies. Primarily because of hanging constraints of computational simplicity and small-sized Gabor masks (7×7, or $9 \times$

9), the design of optimal Gabor filters was not attempted. Although the present work does not address the problem of explicitly designing an optimal filter, our simple filter-selection methodology suggested the best representative filter that performs well in most cases.

IV. UNSUPERVISED WEB INSPECTION

The dimension and orientation of local defects generated in textile webs vary randomly. Therefore, a complete automation of visual inspection process requires unsupervised defect detection that can be used for the online web inspection. The term "unsupervised defect detection" refers to the detection of unknown class of defects for which there is no training. Multichannel filtering theory for the processing of visual information
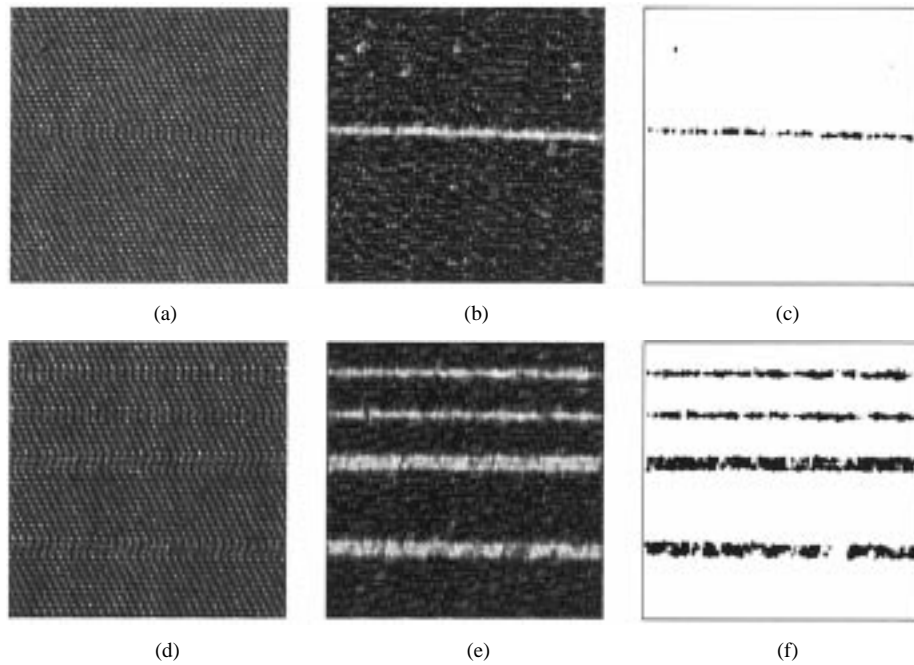
Fig. 4.   Robustness of best representative Gabor filter obtained from the image in Fig. 3(j). Fabric samples with *mispick* in (a) and (d), corresponding filtered images in (b) and (e), and the segmented defects in (c) and (f).

in the biological model of human visual system has inspired various texture segmentation algorithms [27], [32]. A variation of this algorithm, which can be used for the detection of local fabric defects, was presented in [21]. This section investigates another variation of this algorithm using asymmetric Gabor filters described in Section II. Any modification of multichannel filtering algorithm for defect detection should lead to a reduction in computational complexity and, false alarm, and offer high rate of detection.

A. Multichannel Filtering

Unsupervised web inspection requires simultaneous web inspection at local and global scales. Multichannel filtering approach allows multiresolution analysis of fabric texture. The block diagram of this approach is shown in Fig. 5. Every acquired image from the imaging system is filtered with a bank of self-similar Gabor filters detailed in Section II. Each of these Gabor filters is selectively tuned to a narrow range of frequency and orientation. The octave (dyadic) band decomposition is commonly used for wavelet decomposition and was also used in this work for the selection of frequency bands for the frequency-domain sampling of acquired images. The issues relating to the selection of mask size and number of Gabor channels has been discussed in [37]. As a compromise between computational complexity and performance, 18 asymmetric Gabor filters distributed at three scales ($S = 3$) and six orientations ($L = 6$), as shown in Fig. 6, were used in this work. Each of these Gabor filters was implemented as a spatial mask of 7×7 size. Every inspection image $I(x, y)$ is filtered with each of the 18 Gabor filters and the magnitude of every filtered image $I_{pq}^d(x, y)$ is computed using (6).

B. Nonlinearity

Next, a local nonlinear function is used to rectify multichannel filter response. This nonlinear function transforms both
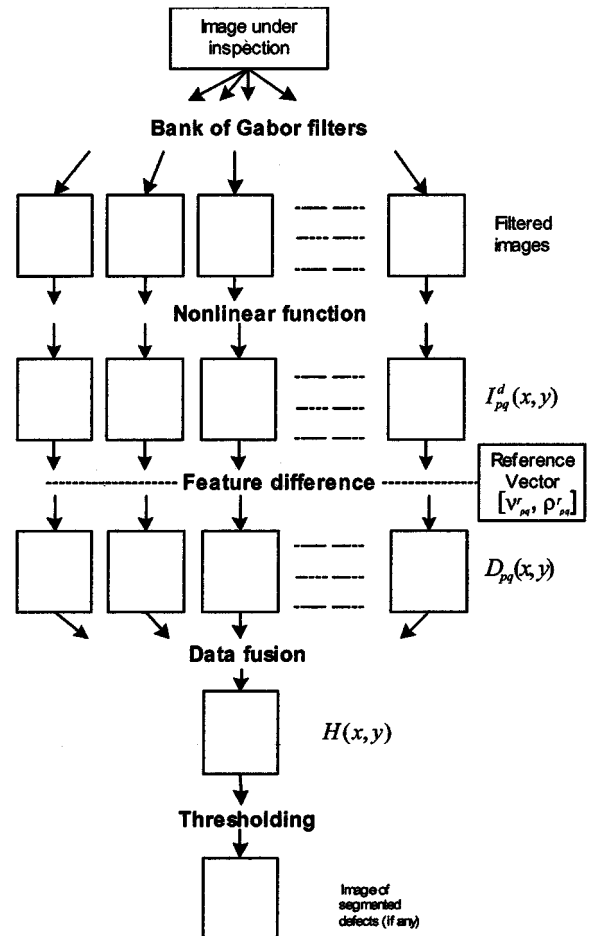

Fig. 5.   Unsupervised defect segmentation in textured materials.

negative and positive amplitudes to positive amplitudes. Reference [26] has a good collection of prior texture segmentation
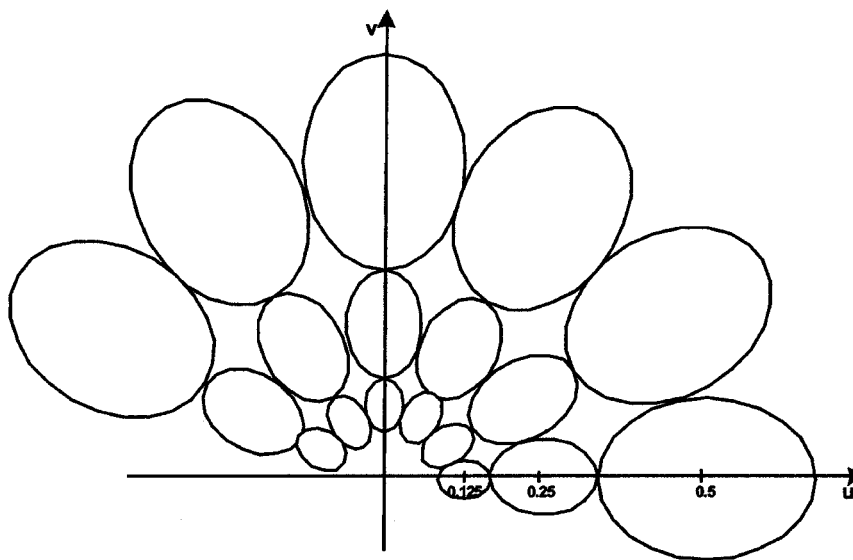
Fig. 6.   Location of 3×6 Gabor filters in spatial-frequency plane.

work using the magnitude $|.|$, the squaring $|.|^2$, and rectified sigmoid $|\tanh(x)|$ nonlinearity. The magnitude nonlinearity requires minimum computations and is, therefore, preferred in this work. This nonlinearity is inherent while computing the magnitude of Gabor filter images (6), therefore, no extra computational burden is added. The 18 images, $I_{pq}^d(x, y)$, represents the features of image under inspection.

C. Feature Difference

An image of defect-free fabric (reference image) is also used to compute 18 reference feature $I_{pq}^r(x, y)$ images, using a procedure similar to that used to obtain $I_{pq}^d(x, y)$. These reference feature images are computed at the beginning of inspection as a part of the calibration operation. The first-order statistics are fundamental for visual characterization of texture [38]. Therefore, the mean (ν_{pq}^r) and standard deviation (ρ_{pq}^r) from each of these 18 images is used to locate defects in the image under inspection. It is now necessary to choose a decision rule for the characterization of pixels in $I_{pq}^d(x, y)$ based on reference features $I_{pq}^r(x, y)$. An optimum decision procedure, in the sense that it has a minimum acceptance region for a given probability of false rejection, has been proposed in [12]. This optimum decision rule [23], which is based on the assumption that features extracted from the reference image is distributed according to multivariate Gaussian distribution, can be simplified as

$$D_{pq}(x, y) = \begin{cases} I_{pq}^d(x, y), & |I_{pq}^d(x, y) - \nu_{pq}^r| \geq \tau.\rho_{pq}^r \\ 0, & \text{otherwise.} \end{cases} \quad (11)$$

The parameter τ determines the sensitivity [22] and is chosen to control the probability of false rejection. An empirically determined value of $\tau = 3$ was found suitable (and used) for the high-resolution inspection images used in this work. The next step is to combine pixels from the difference images $D_{pq}(x, y)$ so as to reduce the probability of false alarm and ensure defect detection in the final image output.

D. Data Fusion

Information gathered by different knowledge sources (channels) from the same image are often uncertain, fuzzy, or incomplete. Several nondeterministic approaches for data fusion using different frameworks have been detailed in [39]. Casasent and Ye [40] have performed qualitative and quantative analyses of several binary and analog fusion algorithms. Bernouli's rule of combination, which is a special case of Dampster's rule of combination, has been used for fabric defect detection in [17] and [22]. Escofect et al. [21] have used: 1) norm vector addition of all pixels at the same scale p (but different directions q) followed by 2) geometric mean of resultant pixel at adjacent scales. This method is attractive because of its computational simplicity and, therefore, a similar approach is pursued here. The following two data fusion schemes were considered for this work:

$$C_q(x, y) = \sum_{p=1}^{S} D_{pq}(x, y)$$

$$H(x, y) = \frac{1}{(L-1)} \left[\sum_{q=1}^{L-1} \{C_q(x, y)C_{q+1}(x, y)\}^{1/2} \right] \quad (12)$$

$$C_p'(x, y) = \sum_{q=1}^{L-1} D_{pq}(x, y)$$

$$H'(x, y) = \frac{1}{(S-1)} \left[\sum_{p=1}^{S-1} \{C_p'(x, y)C_{p+1}'(x, y)\}^{1/2} \right]. \quad (13)$$

The fusion scheme in (12) first generates six images $C_1(x, y), \ldots, C_6(x, y)$ from the addition of pixels at the same scale (p). Then, the geometric mean of resultant pixels at the adjacent orientations generates five images; pixels from these five images are averaged to produce a unique fused image $H(x, y)$. The scheme in (13) is similar to [21], where the vector addition of pixels at the same orientations is computed first.
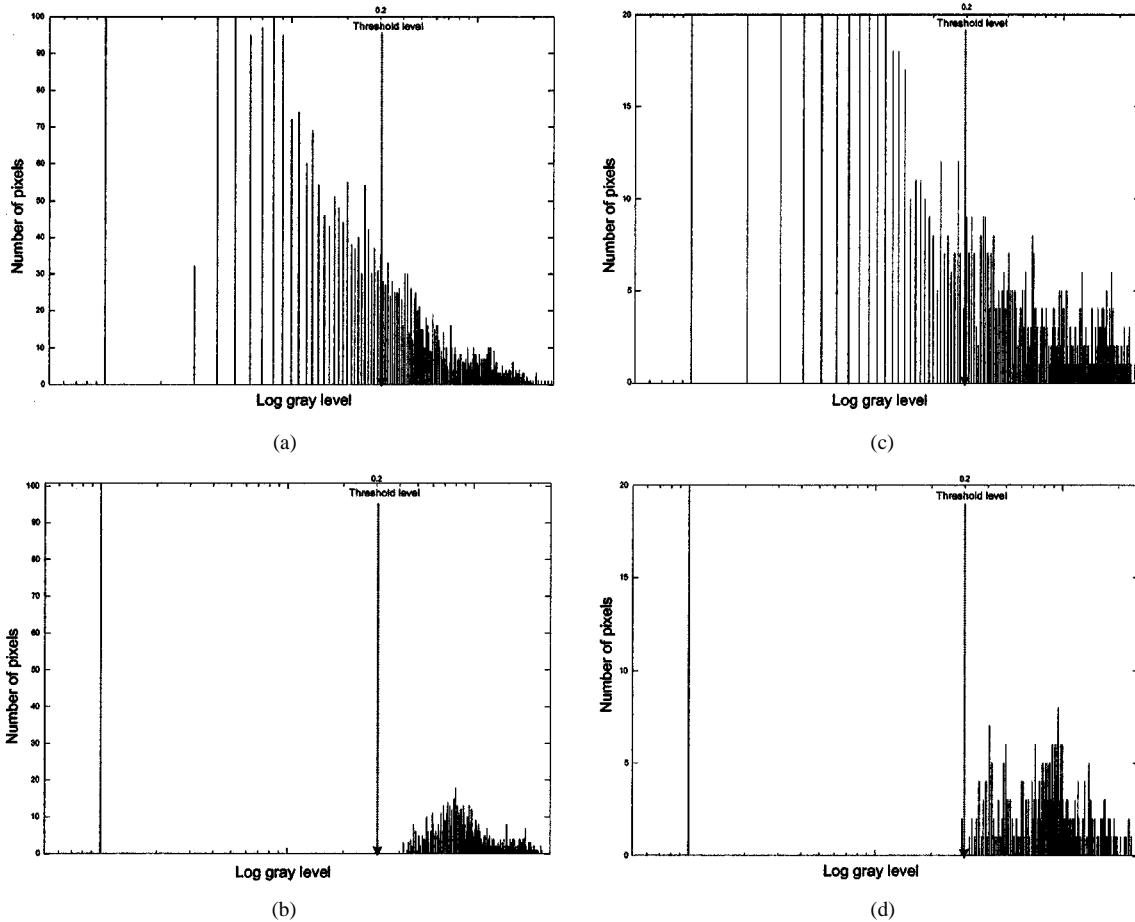
Fig. 7.   Image histograms for $H'(x, y)$ and $H(x, y)$, in (a) and (c), and (b) and (d), respectively. Image shown in Fig. 8(a) is used to obtain histograms in Fig. 7(a) and (b), while the histograms in Fig. 7(c) and (d) are obtained from the image in Fig. 8(b).

While working with both of these schemes, we have found that scheme (12) generates much less noise in the output than the scheme (13) and was, therefore, more suitable[2] for this work. The histograms of the image $H(x, y)$ and $H'(x, y)$ for some of the real fabric samples shown in Fig. 8 are reproduced here in Fig. 7. The image sample with defect *big-knot* [Fig. 8(a)] was used to obtain output images $H(x, y)$ and $H'(x, y)$ separately. The respective gray-level histograms of these two images are shown in Fig. 7(a) and (b). The noise level in the two output images can be seen by observing the number of pixels between zero (0.009 for Fig. 7) and threshold level in the histograms. It can be observed from the histogram in Fig. 7(b) that most of the pixels from the defects are clustered and the noise is nearly zero. However, the results from the same image while using the fusion scheme in (13) have much more noise [Fig. 7(a)] and the thresholding operation is critical for the suppression of noise. A similar set of results, from the image sample with the defect *slack-end* shown in Fig. 8(b), is reproduced in Fig. 7(c) and (d). These results (and subsequent results) suggest that the fusion scheme in (12) works better in the suppression of noise in the output image, than with the fusion scheme in (13). Therefore, the fusion scheme in (12) is used for the further experimental results reported in this paper.

[2]The fusion scheme in (12) cannot be used with the approach in [21], since the Gabor filters at four orientations are nontouching and, therefore, geometric mean of pixels at adjacent orientations is not relevant.

E. Thresholding

The fused image output $H(x, y)$ is subjected to thresholding in order to suppress the pixels not belonging to defect. This operation further reduces the probability of false alarm. The thresholding limit is estimated using the procedure discussed in Section III-B. A reference image (defect free) is used to produce fused image output $H(x, y)_r$ and the thresholding value is computed from this image using (10).

F. Results

The performance of the multichannel filtering scheme described in the above sections was evaluated on fabric samples gathered from a textile loom. The images of plain and twill weave fabric samples, having the same spatial and physical resolution as used in Section III-C, were used for this purpose. The proposed scheme successfully segmented the defects of varying size, orientation, and resolution and, therefore, proved to be robust for online web inspection. The frequency range of the 18 Gabor filters used at three scales was empirically chosen ($f_1 = 1/2$, $f_2 = 1/4$, and $f_3 = 1/8$) as shown in Fig. 6. Some of the twill and plain weave fabric sample images along with their segmented defects are reproduced here in Figs. 8 and 9, respectively.

The segmentation of defects in Figs. 8 and 9 becomes more exact as the mask size is increased from 7×7 to 9×9 or
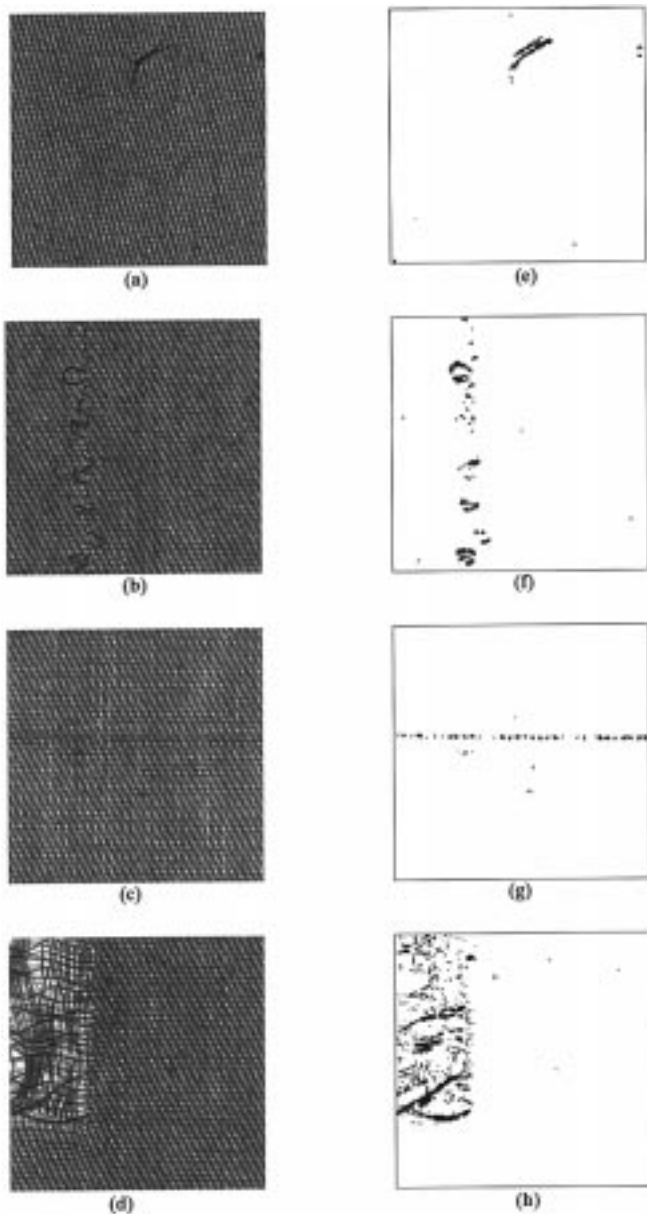
Fig. 8. Twill weave fabric samples with *big-knot*, *slack-end*, *dirty-yarn*, and *netting-multiplies* in (a)–(d), respectively; corresponding segmented defects in (e)–(h).
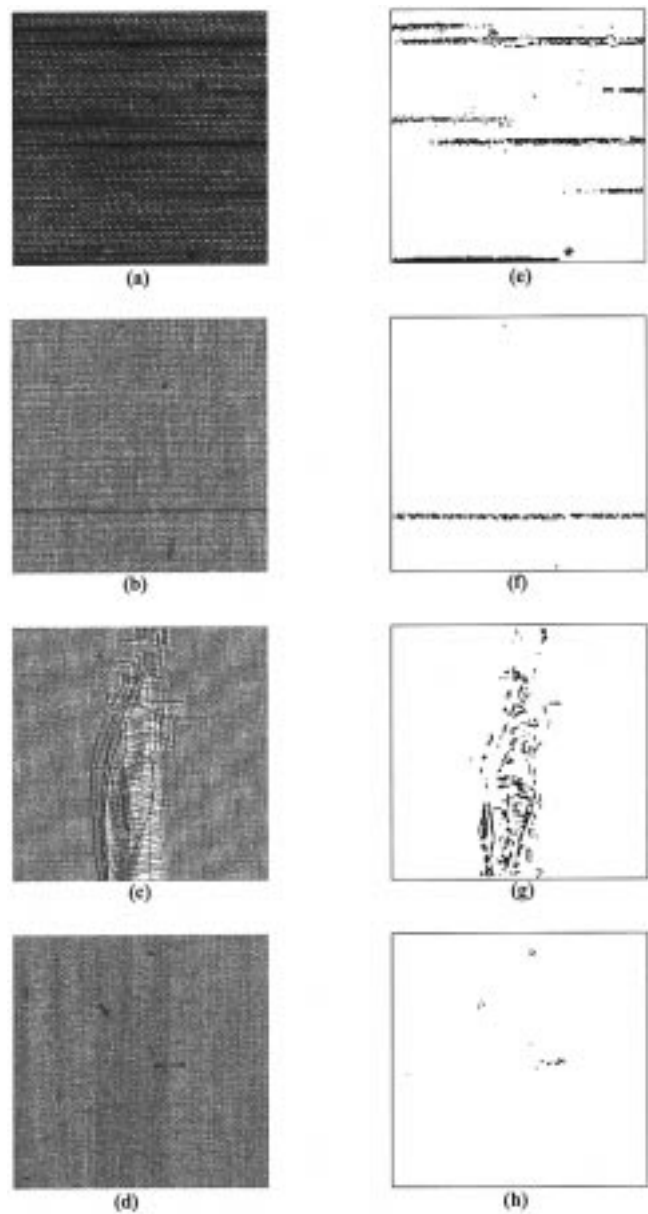
Fig. 9. Plain weave fabric samples with *slubs*, *slack-pick*, *netting-multiplies*, and *kinks* in (a)–(d), respectively; corresponding segmented defects in (e)–(h).

11×11. The choice of the 7×7 mask was only a computational compromise. The frequency range of Gabor filters in the filter bank depends on the range of defects to be detected. Small-sized defects, such as *slack-end*, *dirty-yarn*, *big-knot*, and *slack-pick* shown in Figs. 8 and 9, are better segmented with the Gabor filters centered at higher frequencies (1/2 or 1/4). However, large-sized defects such as *netting-multiplies*, *slubs*, or *oil-stains* have been found to be easily segmented with the Gabor filters centered at lower frequencies. The segmentation of defects such as *netting-multiplies* [Figs. 8(h) and 9(g)] and *slubs* [Fig. 9(e)] was found to be much clearer when frequencies of 18 Gabor filters distributed at ($f_1 = 1/8$, $f_2 = 1/16$, $f_3 = 1/32$). However, this frequency range was not sufficient to give clear segmentation of other small-sized defects shown in Figs. 8 and 9. The frequency range ($f_1 = 1/2$, $f_2 = 1/4$, and

$f_3 = 1/8$) chosen in this work was a compromise to simultaneously detect both large- and small-sized defects appearing on the textile web. A large Gabor filter bank (e.g., with 24 or 28 filters), with a wide range of center frequencies (e.g., from 1/2 to 1/16 or from 1/2 to 1/32), was found to be more robust as it gives the clear and laud segmentation of defects of varying sizes. However, for the reason of computational simplicity, 18 Gabor filters were chosen and the results are demonstrated.

In this work, the frequency range of Gabor filter in the filter bank was determined empirically. However, this range can be suitably determined from the typical range (size) of defects to be segmented from the textile web. The highest center frequency (f_h or f_1) of Gabor filter required can be determined by using the filter selection scheme detailed in Section III-A. This frequency can be determined from the image of a typical fabric

sample having the smallest defect (in either direction) to be segmented. The center frequency of the best representative filter (Section III-A) corresponding to the smallest defect to be segmented should be chosen as (f_h or f_1). Similarly, the frequency of the best representative filter required to segment the largest typical defect in fabric sample can be chosen as (f_l or f_3). The center frequencies of intermediate filters (i.e., f_2) in the filter bank can be heuristically chosen from the computational and performance tradeoff available for the system under implementation.

G. Discussion

Prior work [21] has also demonstrated the application of Gabor filters for fabric defect detection. The approach used in [21] is also another extension of the multichannel filtering scheme used in this work. Two major issues arise in discussing such a defect segmentation scheme: the design of individual filters and the combination/fusion of the filter bank outputs. As compared with the work in [21], there are several differences in this work that have been justified either on computational or performance gain. Firstly, the bank of asymmetric Gabor filters used in this work was chosen such that the half-peak magnitude response of adjacent filters touches each other. The circularly symmetric, nontouching filters used in [21] were modified and more narrowly tuned so that frequency components between the filters are also sampled. Dunn *et al.* [35], [36] have also provided some grounds for the usefulness of nonsymmetric Gabor filters for the texture segmentation, and this was discussed in Section I-B. Secondly, in this work, defect segmentation has been achieved without the usage of low-pass residual images, which required computational intensive operation in [21]. The generation of low-pass-filtered images for every image under inspection required 4 times convolution with cubic B-spline filters (5×5 mask, although separable). In this work, the above computational savings have been achieved while achieving similar results as in [21]. Thirdly, the reduction of Gabor filter mask size from 9×9 in [21] to 7×7 in this work reduces computational load by about 40% in the computation of every Gabor filtered image. Fourthly, a new data fusion scheme has been proposed for combining Gabor filtered images. As detailed in Section IV-D, the fused image output from this scheme gave a better result as compared with the scheme used in [21]. Lastly, the thresholding method suggested in [22] has been used in this work. As detailed in Section III-B, this method does not require any morphological operation that is needed with the thresholding method suggested in [21] and is, therefore, computationally economic.

V. DEFECT DETECTION USING ONLY IMAGINARY GABOR FUNCTION

A multichannel filtering approach for the detection of fabric defects has been presented in the previous section. Despite several efforts to reduce the computational time, real-time implementation of this approach requires additional digital signal processor (DSP) hardware. Low-cost web inspection systems that can run on a simple PC are in increasing demand. Such PC-based systems can perform only limited real-time
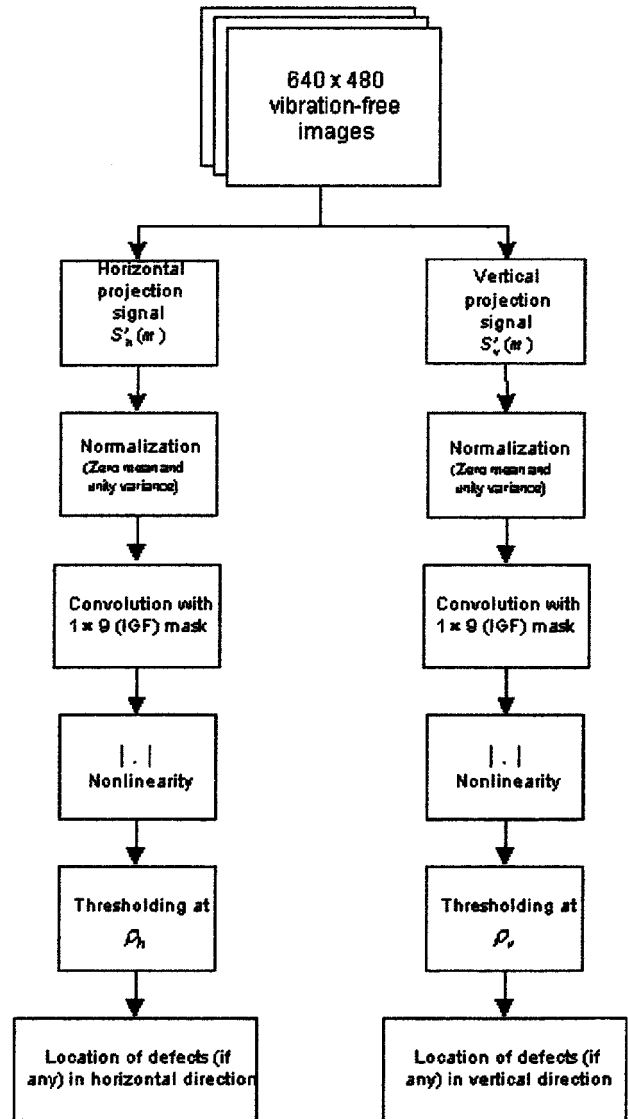

Fig. 10. Block diagram of the proposed defect detection scheme using IGFs.

computations. One possible solution to ease the computational load is to reduce the search space. Due to the nature of weaving process, most of the fabric defects occur either in the vertical or horizontal direction [17]. Thus, the search space can be reduced from a 2-D image to one-dimensional (1-D) signals, obtained from horizontal and vertical projections of pixel values. Kim *et al.* [19] have used such 1-D signals for the detection of fabric defects using Mexican hat wavelet at three scales. In this section, an efficient method of fabric defect detection using only the imaginary part of Gabor function (IGF) is described [37]. In the next sections, this approach is detailed and experimental results are presented.

A. Imaginary Gabor Function

In 1-D, Gabor functions were developed to define signals in both time and frequency domains with minimum uncertainty. In 1-D, odd-symmetric Gabor function (IGF) is given by

$$h(x)_{f, \sigma_x} = \exp\left\{-\frac{1}{2}\left(\frac{x^2}{\sigma_x^2}\right)\right\} \sin(2\pi x f) \qquad (14)$$
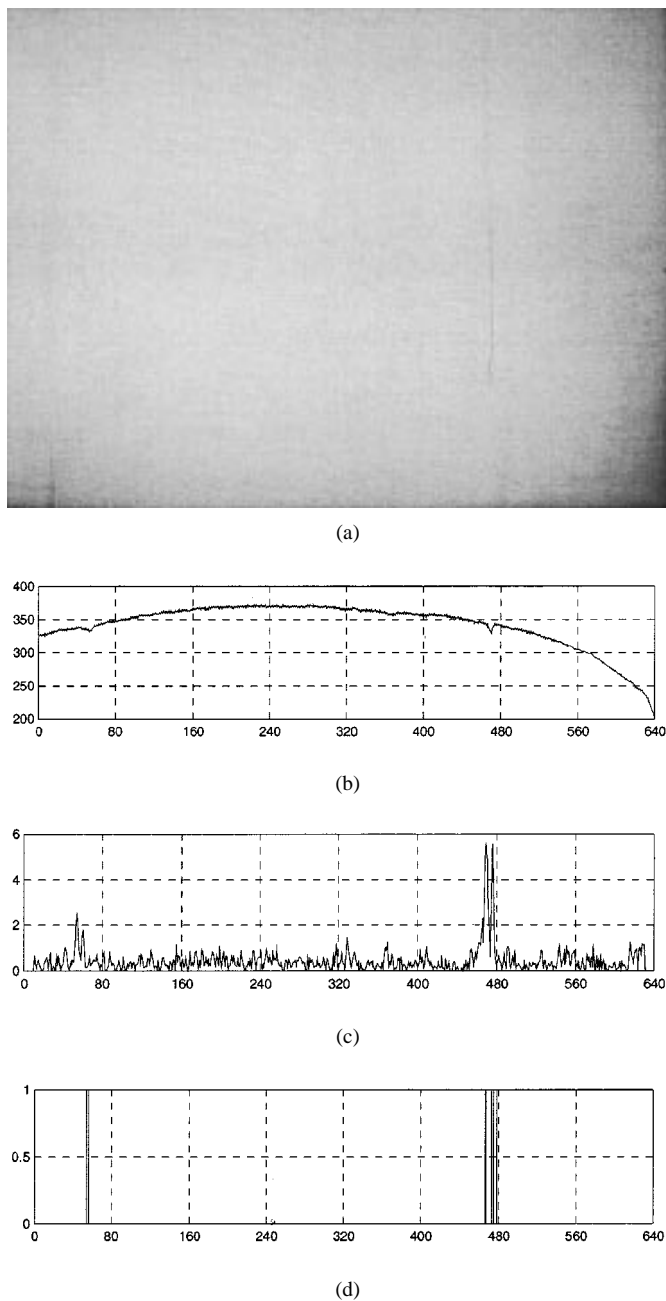
(a)

(b)

(c)

(d)

Fig. 11. (a) Fabric sample with defect *netting-multiplies*. (b) Horizontal projection signal. (c) Convolution of IGF with (b). (d) Defects detected after thresholding.

where f is the frequency of sinusoidal plane wave along the x axis (i.e., the 0° orientation), and σ_x is the space constant of Gaussian envelope. The real part of the 2-D Gabor function acts as a proven blob detector while the imaginary part of the Gabor function acts as a proven edge detector [41]. The IGFs are attractive as edge detectors, since they can be designed to detect both smooth and sharp edge transitions. While analyzing response of Gabor functions with 1-D signal from the fabric defects, we have found that imaginary Gabor function also acts as an edge detector in the 1-D case and is most suitable for detection of defects. The choice $\sigma_x = (3\sqrt{2\ln 2})/(2\pi f)$, that ensures one octave half-peak magnitude bandwidth [22] is used in this work. With the empirical choice of $f = 1/32$, IGFs were implemented as a 1×9 mask.
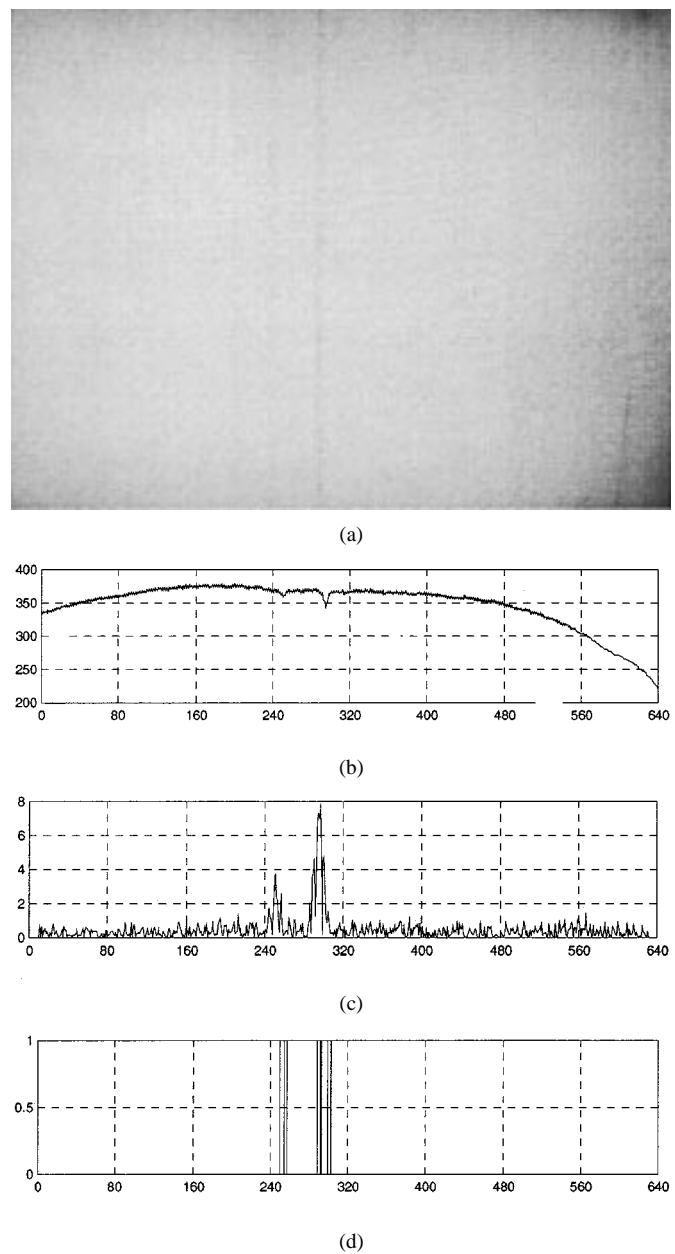

(a)

(b)

(c)

(d)

Fig. 12. Fabric sample with defect *slack-end*, (b) horizontal projection signal, (c) convolution of IGF with (b), (d) defects detected after thresholding.

B. Methodology

The block diagram of the proposed method is shown in Fig. 10. From the vibration-free image $I(m, n)$ of fabric under inspection, as in [19], two 1-D projection signals in each of the horizontal and vertical directions are generated by summing up image pixel values along columns and rows, respectively,

$$s'_h(n) = \sum_{m=1}^{M} I(m, n)$$

$$s'_v(m) = \sum_{n=1}^{N} I(m, n)$$

$$s_h(n) = \frac{1}{\sigma_h} \{s'_h(n) - \mu_h\}$$

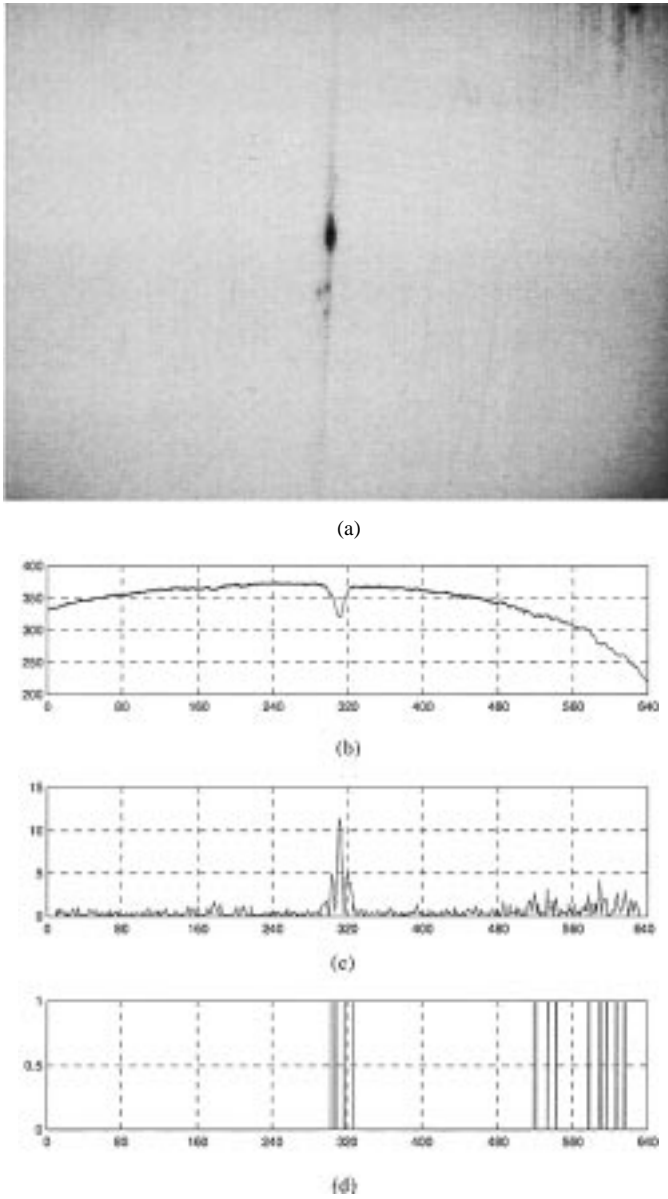$$s'_v(m) = \frac{1}{\sigma_v} \{s'_v(m) - \mu_v\}. \tag{15}$$

Fig. 13.   (a) Fabric sample with defect *dirty-yarn*. (b) Horizontal projection signal. (c) Convolution of IGF with (b). (d) Detected defect after thresholding.

μ_h and μ_v are the mean values of signal $s'_h(n)$ and $s'_v(m)$, respectively, and are used to make $s_h(m)$ and $s_v(n)$ zero mean. Similarly, σ_h and σ_v are the variance of signal $s'_h(n)$ and $s'_v(m)$, respectively, and are used to make $s_h(m)$ and $s_v(n)$ of unity variance. The 1-D signals $s_h(m)$ and $s_v(n)$ are filtered with IGF masks (Section V-A) and, thus, two new signals $f_h(n)$ and $f_v(m)$ are generated

$$f_h(n) = |h(x) * s_h(n)| = \left| \sum_{l=1}^{N} s_h(l)h(x-l) \right|$$

$$f_v(m) = |h(x) * s_v(m)| = \left| \sum_{k=1}^{M} s_v(k)h(x-k) \right|. \quad (16)$$

These signals are subjected to the thresholding operation and the resultant signal shows the location of defects in the fabric.
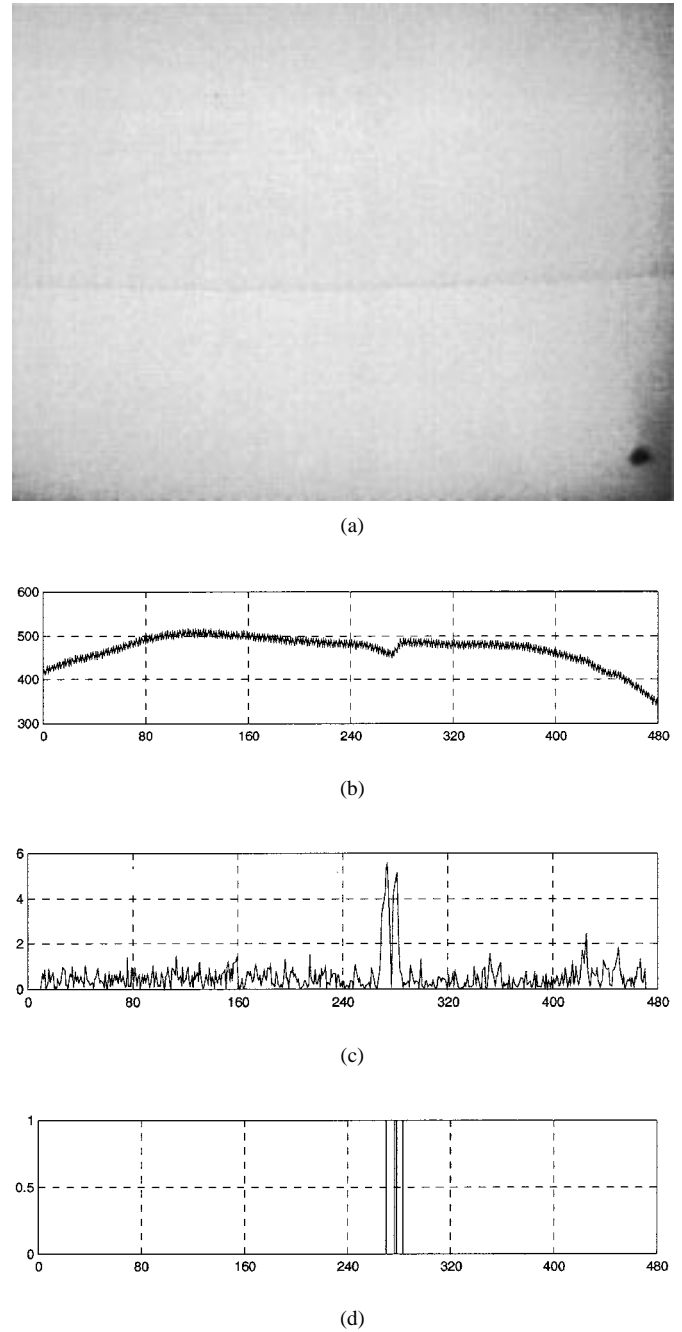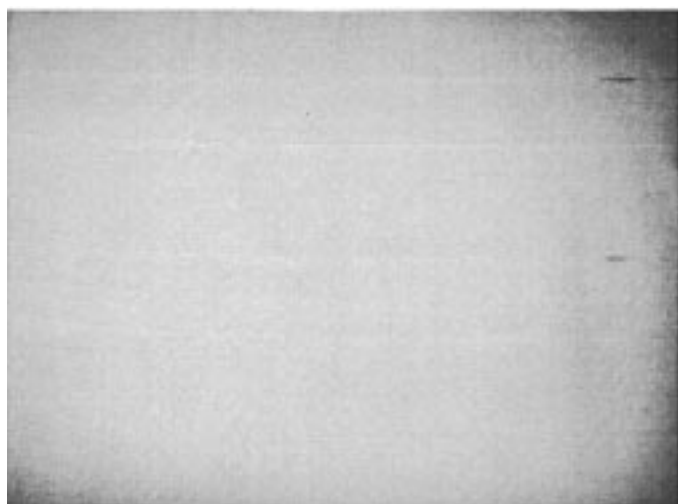

Fig. 14.   (a) Fabric sample with defect *thick-bar*. (b) Vertical projection signal. (c) Convolution with IGF. (d) Detected defect after thresholding.

The thresholding value is computed from a reference (defect free) fabric sample. From this reference fabric image, $f_{h_{\mathrm{ref}}}(n)$ and $f_{v_{\mathrm{ref}}}(m)$ using (15) and (16) are generated. The thresholding value for each of the horizontal and vertical directions is generated as follows [37]:

$$\rho_h = \max_{m \in R} \{f_{h_{\mathrm{ref}}}(n)\} \quad \rho_v = \max_{n \in R} \{f_{v_{\mathrm{ref}}}(m)\} \quad (17)$$
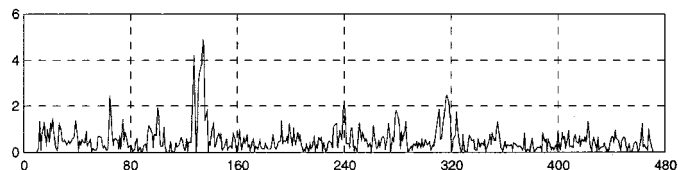
where "R" is a window centered at the signal. Thus, the threshold value ρ_h is the maximum amplitude of signal, within a window "R," in the signal $f_{h_{\mathrm{ref}}}(n)$ obtained from the reference image. The window size is chosen to avoid the effect
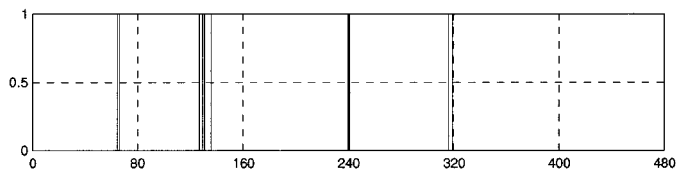
(a)
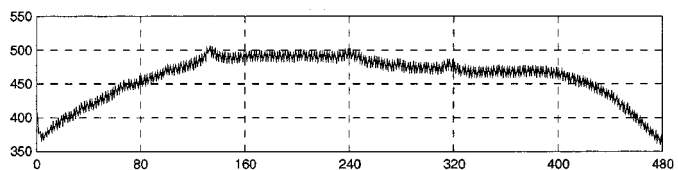
(b)

(c)

(d)

Fig. 15.   (a) Fabric sample with defect *mispick*. (b) Vertical projection signal. (c) Convolution of IGF with (b). (d) Detected defect after thresholding.
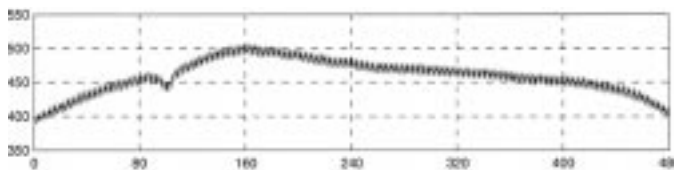

(a)

(b)

(c)

(d)

Fig. 16.   Fabric sample with defect *shuttle-mark*. (b) Vertical projection signal. (c) Convolution with IGF (b). (d) Detected defect after thresholding.

from border distortion. This can be was obtained by removing at least 9 pixels from each side of the signal $f_{h_{\text{ref}}}(v)$ when a 1×9 mask is used.
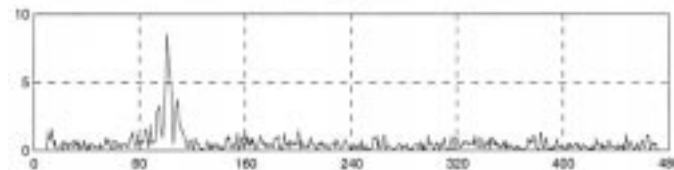
C. Experimental Setup and Results

For increased throughput, low-resolution images of about 45 pixels/in (640 pixels cover 14 in of fabric) are used so that larger fabric area per frame can be processed. Using an Ominivision digital OV7110 camera with 640×480 pixels, vibration-free black-and-white images of fabric under inspection are acquired under backlighting. The experimental results with these images were excellent and some of these results are reproduced in Figs. 11–16, and summarized in Table I.

Fig. 11(a) shows a fabric sample image with defect *netting-multiplies*. A 1×9 IGF mask is convolved with $s_h(n)$ signal generated from this image. As seen in Fig. 11(b), IGF mask enhances the signal at locations corresponding to the defects. Since the IGF has zero mean and the nonlinearity in (16) is even-symmetric, both light and dark edges are equally detected [37]. In Fig. 11(d), the thresholding operation segments the location of signal corresponding to defect. Similarly, detection results for fabric samples with *slack-end* and *dirty-yarn* are reproduced in Figs. 12 and 13, respectively. In order to avoid border-effect distortion, the first and last 10 pixels have been discarded from the signal $s_h(n)$ [and $s_v(m)$]. For fabric samples in Figs. 11–13, there is no detection of defects from the vertical projection signal $s'_v(m)$. Therefore, results from the vertical projection signal are not shown for these images. As seen

TABLE I
DEFECT DETECTION RESULTS FROM THE PROPOSED METHOD IN SECTION V

S.No.	Name of the defect	Result from Horizontal projection	Results from vertical projection	Comments
1.	*Netting-multiplies*	Full detection	No detection	Figure 11
2.	*Slack-end*	Full detection	No detection	Figure 12
3.	*Dirty-yarn*	Full detection	No detection	Figure 13
4.	*Thick-bar*	No detection	Full detection	Figure 14
5.	*Mispick*	No detection	Full detection	Figure 15
6.	*Shuttle-mark*	No detection	Full detection	Figure 16
7.	*Wavy-face*	No detection	Full detection	
8.	*Wrong-draw*	Partial detection	No detection	Very small (subtle) defect, therefore partial detection.
9.	*Thin-bar*	No detection	Full detection	
10.	*Thick-yarn*	Full detection	No detection	
11.	*Oil-stain*	Partial detection	Full detection	
12.	*Break-out*	Detection with false alarm	Full detection	False alarm, because of creases in the image.
13.	*Kink*	Partial detection	Full detection	

from the results in Figs. 11–13, the defects have been detected quite accurately.

Figs. 14–16 shows fabric samples and detection results for *thick-bar*, *mispick*, and *shuttle-mark*, respectively. As can be seen from the Table I, defects in these images can only be detected from vertical projection signal $s'_v(m)$ and, therefore, results from horizontal projection signal $s'_h(n)$ are not shown. Results from some other common fabric defects, whose figures are not shown in this paper, are summarized in Table I. Some of the blob-shaped defects like *oil-stain* and *shuttle-mark* were also detected, since the defect boundaries in the projection signal $s'_h(n)$ and $s'_v(m)$ form edges. The computational time of this algorithm as run on a Pentium III 450 MHz PC using a simple C program is 94 ms. Therefore, no additional DSP hardware is required for online inspection using the proposed algorithm.

D. Discussion

Our experimental results have suggested that detecting fabric defects with 1-D projection signals becomes harder as the size of the defects increases. As seen from the results in Fig. 14 and 16, small blobs (near corners), which fail to form any subtle change in projection signals, have not been detected. The creases (wrinkles) in fabric under inspection are detected as defects and, therefore, generate a false alarm. Therefore, the imaging system has to adjusted in such a way as to avoid wrinkles in the low-resolution images. Another observation from the experimental results is that the distortion introduced due to uneven illumination of the images does not have any effect on detection. The effects of uneven illumination can be observed from projection signals [$s'_h(n)$ and $s'_v(m)$]. The low-frequency distortion signal, superimposed on the high-frequency signal, has not generated any problem (i.e., false alarm) in the detection of defects. This is due to the fact that the IGF is zero mean and, hence, insensitive to background illumination. The real part of the Gabor function (RGF), which acts as a blob detector, is not zero mean and, hence, is sensitive to background illumination. Although

the RGF is ideal for detecting blobs (e.g., Figs. 13 and 16) and large-sized defects from the 1-D signal, it is not used in the proposed defect detection method since its usage requires high-resolution images, which would increase the cost of the system.

VI. CONCLUSIONS

In this paper, a supervised defect detection approach to detect a class of fabric defects has been demonstrated. The multichannel filtering scheme, hitherto used for texture segmentation, has been extended and tailored for unsupervised inspection of textile webs. The role of mask size, and the number and frequency range of Gabor filters in the filter bank, on performance and computational load has been discussed. A user can appropriately select these parameters depending on the tradeoff available in his or her system, between performance and computational load. The results in this paper have shown that this scheme is robust and ready to be used for online web inspection.

The online unsupervised inspection using the multichannel filtering scheme requires additional DSP hardware. Therefore, a low-cost inspection solution based on edge detection with IGF has been developed for fabric defect detection. The performance of this method has been extensively evaluated on a variety of fabric defects. The results have shown that this method is quite successful and offers a low-cost single-PC-based solution for online web inspection. From the various experiments conducted on web inspection (discussed above), five important factors on the success of real-time defect detection schemes can be outlined. These are" 1) contrast associated with a defect; 2) consistency of background; 3) image resolution; 4) size of defect to be detected; and 5) speed of inspection. While 1) and 2) are affected by illumination conditions, factor 3) depends on field of view and resolution of CMOS or charge-coupled-device (CCD) photosensor used for imaging. The computational complexity of this method can be approximated as two opera-

tions per pixel, which are due to the computations involved in the generation of two projection signals. Although the results of the proposed schemes have been demonstrated, for the fabric inspection, these schemes can potentially be used for online inspection of other textured materials such as steel rolls, plastic, or wood.

REFERENCES

[1] D. Brzakovic and H. Sari-Sarraf, "Automated inspection of nonwoven web materials: A case study," *Proc. SPIE*, vol. 2183, pp. 214–222, Feb. 1994.
[2] J. W. Roberts, S. D. Rose, G. A. Jullian, G. A. Nichols, L. Jenkins, P. Chamberlain, and S. G. Maroscher, "PC based real-time defect imaging system for high speed web inspection," *Proc. SPIE*, vol. 1907, pp. 164–176, Feb. 1993.
[3] J. Laitinen, "Image quality in automated visual web inspection," *Proc. SPIE*, vol. 3029, pp. 78–89, Apr. 1997.
[4] R. W. Conners, C. W. McMillin, K. Lin, and R. E. Vasquez-Espinosa, "Identifying and locating surface defects in wood: Part of an automated lumber processing system," *IEEE Trans. Pattern Anal. Machine Intell.*, vol. 5, pp. 573–583, Nov. 1983.
[5] E. Young, "Use of line scan cameras and a DSP processing system for high-speed wood inspection," *Proc. SPIE*, vol. 2597, pp. 259–264, Oct. 1995.
[6] L. Siew, R. M. Hodgson, and E. J. Wood, "Texture measures for carpet wear assessment," *IEEE Trans. Pattern Anal. Machine Intell.*, vol. 10, pp. 92–105, Jan. 1988.
[7] S. H. Sheen, H. T. Chien, W. P. Lawrence, and A. C. Raptis, "Ultrasonic imaging system for in-process fabric defect detection," U.S. Patent 5 665 907, Sept. 1997.
[8] L. Dorrity and G. Vachtsevanos, "In-process fabric defect detection and identification," presented at the Mechatronics'98, Skovde, Sweden, Sept. 1998.
[9] I.-S. Tsai, Ch.-H. Lin, and J.-J. Lin, "Applying an artificial neural network to pattern recognition," *Textile Res. J.*, vol. 65, pp. 123–130, Mar. 1995.
[10] X. F. Zhang and R. R. Bresee, "Fabric defect detection and classification using image analysis," *Textile Res. J.*, vol. 65, no. 1, pp. 1–9, 1995.
[11] E. J. Wood, "Applying Fourier and associated transforms to pattern characterization in textiles," *Textile Res. J.*, vol. 60, no. Apr., pp. 212–220, 1990.
[12] M. Unser and F. Ade, "Feature extraction and decision procedure for automated inspection of textured materials," *Pattern Recognit. Lett.*, vol. 2, pp. 181–191, Mar. 1984.
[13] F. S. Cohen, Z. Fau, and S. Attali, "Automated inspection of textile fabrics using textured models," *IEEE Trans. Pattern Anal. Machine Intell.*, vol. 13, pp. 803–808, Aug. 1991.
[14] J. G. Campbell, C. Fraley, F. Murtagh, and A. E. Raftery, "Linear flaw detection in woven textiles using model-based clustering," *Pattern Recognit. Lett.*, vol. 18, pp. 1539–1548, 1997.
[15] S. A. Hosseini Ravindi, "Fourier transform analysis of plain weave fabric appearance," *Textile Res. J.*, vol. 65, pp. 676–683, Nov. 1995.
[16] C. H. Chan and G. Pang, "Fabric defect detection by Fourier analysis," *IEEE Trans. Ind. Applicat.*, vol. 36, pp. 1267–1276, Sept./Oct. 2000.
[17] H. Sari-Sarraf and J. S. Goddard, "Vision systems for on-loom fabric inspection," *IEEE Trans. Ind. Applicat.*, vol. 35, pp. 1252–1259, Nov./Dec. 1999.
[18] J. G. Vachtsevanos, M. Mufti, and J. L. Dorrity, "Method and apparatus for analyzing an image to detect and identify defects," U.S. Patent 5 815 198, Sept. 1998.
[19] S. Kim, M. H. Lee, and K. B. Woo, "Wavelet analysis to defects detection in weaving processes," in *Proc. IEEE Int. Symp. Industrial Electronics*, vol. 3, July 1999, pp. 1406–1409.
[20] W. J. Jasper, S. J. Garnier, and H. Potapalli, "Texture characterization and defect detection using adaptive wavelets," *Opt. Eng.*, vol. 35, pp. 3140–3149, Nov. 1996.
[21] J. Escofet, R. Navarro, M. S. Millan, and J. Pladelloreans, "Detection of local defects in textiles webs using Gabor filters," *Opt. Eng.*, vol. 37, pp. 2297–2307, Aug. 1998.
[22] A. Kumar and G. Pang, "Fabric defect segmentation using multichannel blob detectors," *Opt. Eng.*, vol. 39, no. 12, pp. 3176–3190, Dec. 2000.

[23] F. Ade, N. Lins, and M. Unser, "Comparison of various filter sets for defect detection in textiles," in *Proc. 7th Int. Conf. Pattern Recognition*, vol. 1, Montreal, QC, Canada, 1984, pp. 428–431.
[24] S. Mallat, "Wavelets for a vision," *Proc. IEEE*, vol. 84, pp. 604–614, Apr. 1996.
[25] J. Daugman, "Uncertainty relation for resolution in space, spatial frequency, and orientation optimized by two-dimensional visual cortical filters," *J. Opt. Soc. Amer.*, vol. 2, no. 7, pp. 1160–1169, 1985.
[26] T. Randen and J. H. Husøy, "Filtering for texture classification: A comparative study," *IEEE Trans. Pattern Anal. Machine Intell.*, vol. 21, pp. 291–310, Apr. 1999.
[27] B. S. Manjunath and W. Y. Ma, "Texture features for browsing and retrieval of image data," *IEEE Trans. Pattern Anal. Machine Intell.*, vol. 18, no. 8, pp. 837–842, Aug. 1996.
[28] H. W. Tang, V. Srinivasan, and S. H. Ong, "Texture segmentation via nonlinear interactions among Gabor feature pairs," *Opt. Eng.*, vol. 34, pp. 125–134, Jan. 1995.
[29] B. S. Manjunath and W. Y. Ma, "Texture features for browsing and retrieval of image data," Dept. Elect. Comput. Eng., Univ. California, Santa Barbara, Tech. Rep. CIPR TR 95-06, June 1995.
[30] A. K. Jain and S. Bhattacharjee, "Text segmentation using Gabor filters for automatic document processing," *Mach. Vis. Appl.*, vol. 5, pp. 169–184, 1992.
[31] D. F. Dunn, T. P. Weldon, and W. E. Higgins, "Extracting halftones from printed documents using texture analysis," *Opt. Eng.*, vol. 36, pp. 1044–1052, Apr. 1997.
[32] A. K. Jain, N. L. Ratha, and S. Lakshmanan, "Object detection using Gabor filters," *Pattern Recognit.*, vol. 30, pp. 295–309, Feb. 1987.
[33] J. Sklansky, "Image segmentation and feature extraction," *IEEE Trans. Syst., Man, Cybern.*, vol. 8, pp. 237–247, Apr. 1978.
[34] A. R. Rao, *A Taxonomy for Texture Description and Identification*. New York: Springer-Verlag, 1990.
[35] D. Dunn, W. E. Higgins, and J. Wakeley, "Texture segmentation using 2-D Gabor elementary functions," *IEEE Trans. Pattern Anal. Machine Intell.*, vol. 16, pp. 130–148, Feb. 1994.
[36] D. Dunn and W. E. Higgins, "Optimal Gabor filters for texture segmentation," *IEEE Trans. Image Processing*, vol. 4, pp. 947–963, July 1995.
[37] A. Kumar, "Automated defect detection in textured materials," Ph.D. dissertation, Dept. Elect. Electron. Eng., The Univ. Hong Kong, Hong Kong, May 2001.
[38] B. Julsez, "Visual pattern discrimination," *IRE Trans. Inform. Theory*, vol. 8, pp. 84–92, 1962.
[39] M. Abdulghafour, J. Goddard, and M. A. Abidi, "Non-deterministic approaches in data fusion—A review," *Proc. SPIE*, vol. 1393, pp. 596–610, Nov. 1990.
[40] D. Casasent and A. Ye, "Detection filters and algorithm fusion for ATR," *IEEE Trans. Image Processing*, vol. 6, pp. 114–125, Jan. 1997.
[41] D. Casasent and J. S. Smokelin, "Real, imaginary, and clutter Gabor filter fusion for detection with reduced false alarms," *Opt. Eng.*, vol. 33, no. 7, pp. 2255–2363, Jul. 1994.

Ajay Kumar (S'99–M'01) received the Ph.D. degree from The University of Hong Kong, Hong Kong, in 2001.

He was with Indian Institute of Technology, Kanpur, India, as a Junior Research Fellow and with Indian Institute of Technology, Delhi, India, as a Senior Scientific Officer prior to joining Indian Railways. In 1993, he joined the Indian Railway Service of Signal Engineers (IRSSE) as an Assistant Signal and Telecom Engineer. He was a Project Engineer with Indian Institute of Technology, Kanpur, from 1996 to 1997 and an Assistant Professor at NIST, Berhampur, India, from September 1997 to September 1998. He was a Research Associate with The University of Hong Kong from December 1998 to August 1999. He is currently engaged in his postdoctoral research in the Department of Computer Science, Hong Kong University of Science and Technology, Hong Kong. His research interests include pattern recognition with an emphasis on biometrics and defect detection using wavelets, filter banks, general texture analysis, and neural networks.

Dr. Kumar was an Executive Council Member of The University of Hong Kong IEEE Students Branch from 1999 to 2000.

Grantham K. H. Pang (S'84–M'86–SM'01) received the Ph.D. degree from the University of Cambridge, Cambridge, U.K., in 1986 for research in multivariable control system design and expert systems.

He was with the Department of Electrical and Computer Engineering, University of Waterloo, Waterloo, ON, Canada, from 1986 to 1996. He joined the Department of Electrical and Electronic Engineering, The University of Hong Kong, Hong Kong, in 1996. Since 1988, he has authored more than 80 published technical papers and has authored or coauthored three books. His research interests include expert systems for control system design, intelligent control, intelligent transportation systems, neural networks, control theory, and computer-aided design. In 1994, he was a Senior Visiting Researcher at Hitachi Research Laboratory, Japan. He has acted as a Consultant to many companies, including Mitsubishi Electric Corporation, Japan, and Northern Telecom and Imperial Oil Ltd., Canada. He is an Editor of the *International Journal of Intelligent Control and Systems* and *Control and Computers*, published by the International Association of Science and Technology for Development (IASTED).

Dr. Pang was the Organizing Chair of the 1996 IEEE Symposium on Computer-Aided Control System Design. He was appointed by the President of the IEEE Control Systems Society as the Chair of the Technical Committee on Computer-Aided Control System Design (1993–1995). In 1989, he was awarded the ICI Prize for authorship of the best paper on the application of the theory of control published in the *Transactions of the Institute of Measurement and Control*. He is a Chartered Electrical Engineer in the U.K. and a member of the Institution of Electrical Engineers, U.K., and Hong Kong Institution of Engineers.